Local artifacts in ice core methane records caused by layered bubble trapping and in-situ production: a multi-site investigation

Rachael H. Rhodes [1*], **Xavier Faïn** [2], **Edward J. Brook** [1], **Joseph R. McConnell** [3], **Olivia J. Maselli** [3], **Michael Sigl** [3,4], **Jon Edwards** [1], **Christo Buizert** [1], **Thomas Blunier** [5], **Jérôme Chappellaz** [2], **Johannes Freitag** [6]

[1] {College of Earth, Ocean and Atmospheric Sciences, Oregon State University, Corvallis OR, USA}

[2] {Université Grenoble Alpes/CNRS, Laboratoire de Glaciologie et Géophysique de l'Environnement, Grenoble, France}

[3] {Division of Hydrologic Sciences, Desert Research Institute, Reno NV, USA

[4] {Laboratory for Radiochemistry and Environmental Chemistry, Paul Scherrer Institut, Villigen, Switzerland}

[5] {Centre for Ice and Climate, Niels Bohr Institute, University of Copenhagen, Copenhagen Denmark}

[6] {Alfred Wegener Institute, Helmholtz Centre for Polar and Marine Research, Bremerhaven, Germany}

[*] {now at Department of Earth Sciences, University of Cambridge, Cambridge, UK}

Correspondence to: R. H. Rhodes (rhr34@cam.ac.uk)

Abstract

Advances in trace gas analysis allow localised, non-atmospheric features to be resolved in ice cores, superimposed on the coherent atmospheric signal. These high frequency signals could not have survived the low-pass filter effect that firn diffusion exerts on the atmospheric history and therefore do not result from changes in the atmospheric composition at the ice sheet surface. Using continuous methane (CH_4) records obtained from five polar ice cores, we characterize these non-atmospheric signals and explore their origin. Isolated samples, enriched in CH_4 in the Tunu13 (Greenland) record are linked to the presence of melt layers. Melting can enrich the methane concentration due to a solubility effect, but we find that an additional in-situ process is required to generate the full magnitude of these anomalies. Furthermore, in the all ice cores studied there is evidence of reproducible, decimetre-scale CH_4 variability. Through a series of tests, we demonstrate that this is an artifact of layered bubble trapping in a heterogeneous-density firn column; we use the term 'trapping signal' for this phenomenon. The peak-to-peak amplitude of the trapping signal is typically 5 ppb, but may exceed 40 ppb. Signal magnitude increases with atmospheric CH_4 growth rate and seasonal density contrast, and decreases with accumulation rate. Significant annual periodicity is present in the CH_4 variability of two Greenland ice cores, suggesting that layered gas trapping at these sites is controlled by regular, seasonal variations in the physical properties of the firn. Future analytical campaigns should anticipate high frequency artifacts at high-melt ice core sites or during time periods with high atmospheric CH_4 growth rate in order to avoid misinterpretation of such features as past changes in atmospheric composition.

1 Introduction

Continuous measurement of ice core methane (CH_4) concentrations utilising laser spectroscopy (Stowasser et al., 2012) is rapidly emerging as a powerful tool in palaeoclimatology, producing highly detailed records of atmospheric methane for the Last Glacial Period (Chappellaz et al., 2013; Rhodes et al., 2015) and Late Holocene (Rhodes et al., 2013). The ability to expediently and precisely measure trace gases in ice cores at centimetre-scale depth resolution also allows us to locally resolve novel, high frequency signals that do not reflect past atmospheric conditions (Faïn et al., 2014; Rhodes et al., 2013) but instead reveal new information about other processes that influence trace gases in ice cores.

The processes of diffusive mixing and gradual bubble close-off, which occur in the firn column, cumulatively act as a low-pass filter, removing high frequency atmospheric signals, such as the CH_4 seasonal cycle (Schwander et al., 1993; Trudinger et al., 1997). All polar ice cores therefore yield trace gas records that are smoothed versions of the actual atmospheric history, with the degree of smoothing depending on site conditions, particularly temperature and accumulation rate (Schwander et al., 1997). Although the degree to which any atmospheric signal is damped by the firn is not always well constrained in the past, it can be estimated (Rosen et al., 2014; Spahni et al., 2003). Trace gas signals present at frequencies above those that could be preserved in the face of the natural smoothing cannot represent atmospheric history. If they are present we must assume that they are not related directly to the original atmospheric variation at the surface of the ice sheet.

A previous study of Late Holocene Greenlandic ice (North Greenland Eemian Project (NEEM)-2011-S1 ice core) (Rhodes et al., 2013) identified three categories of non-atmospheric CH_4 signals:

       1) *Infrequent, abrupt CH_4 spikes (20-100 cm depth interval, 35-80 ppb excess CH_4) coincident with elevated concentrations of refractory black carbon and ammonium (NH_4^+), suggested to be linked to microbial in-situ production.* Similar amplitude CH_4 anomalies, typically coeval with elevated NH_4^+, were subsequently reported in Greenland Ice Sheet Project 2 (GISP2) Holocene ice (Mitchell et al., 2013). The NEEM Community

1   Members (2013) also implicated biological in-situ production in the much larger

2   amplitude (> 1000 ppb) CH_4 anomalies observed in NEEM ice dating from the last

3   interglacial (Eemian).

4   2) *CH_4 oscillations of > 100 ppb peak-to-peak amplitude through the lock-in zone.*

5   Following Etheridge et al. (1992), it was suggested that the CH_4 variability was related to

6   the mechanism of layered bubble trapping (Fig. 1). Briefly, according to this mechanism,

7   air bubbles in relatively dense layers close off earlier, trapping anomalously old air, and

8   air bubbles in less dense layers close off later, trapping relatively young air. Providing

9   that there is a sustained gradient of change in atmospheric methane across this time span,

10   the air bubbles in adjacent layers will contain different concentrations of methane.

11   Mitchell et al. (2015) quantified this phenomenon in samples from the lock-in zone of the

12   West Antarctic Ice Sheet (WAIS)-Divide ice core and developed a parameterisation for

13   layered bubble trapping in a firn densification model.

14   3) *Quasi-annual scale CH_4 oscillations of 24 ppb peak-to-peak amplitude in the*

15   *mature ice phase.* Such features had only been observed previously in mature ice at Law

16   Dome by Etheridge et al. (1992) who observed CH_4 variability consistent with younger

17   air being trapped in summer layers and older air trapped in winter layers. Although

18   Rhodes et al. (2013) hypothesized that they observed similar features, decimetre scale

19   CH_4 oscillations were observed throughout the NEEM-2011-S1 CH_4 record, not only

20   during periods of sustained change in atmospheric CH_4 concentration, questioning

21   whether all the resolved variability could be attributed to the layered bubble trapping

22   mechanism.

23   The findings summarised above generate many questions about what factors affect the

24   biological and/or physical mechanisms responsible for the non-atmospheric CH_4 signals

25   in polar glacial ice. For example, is the suspected in-situ production of CH_4 ubiquitous

26   across the Greenland ice sheet? Can similar anomalous signals be detected in Antarctic

27   ice that has a significantly lower impurity loading? How do site temperature,

28   accumulation rate and impurity load affect the high frequency CH_4 variability tentatively

29   linked to layered bubble close-off?

These questions are critically important because ice core trace gas records are integral to palaeoclimatology, enabling us to investigate the relationship between atmospheric greenhouse gases and climate prior to the late 20th century. Recent analytical advances in both discrete (Mitchell et al., 2011) and continuous trace gas measurement techniques (Rhodes et al., 2013; Stowasser et al., 2012) have increased data precision and resolution, which is undoubtedly advantageous for palaeoclimate research, but also increases the likelihood of resolving non-atmospheric signals. Avoiding misinterpretation of non-atmospheric signals and therefore having confidence in the fidelity of the atmospheric histories constructed from ice cores requires detailed knowledge of the physical and biological processes that may locally affect trace gas records. This knowledge, acquired from polar ice cores, could also provide hints about how to extract an atmospheric signal from gas measurements performed on non-polar ice cores that are significantly affects by such artifacts (e.g., Hou et al., 2013). Furthermore, by studying non-atmospheric artifacts in ice core gas records we may learn about the physical mechanisms which trap air bubbles in the firn enabling us to improve numerical model parameterisations used to estimate the gas age-ice age difference and the smoothing effect of firn-based processes. Additionally, it may be possible to glean information about biological activity in one of the harshest biomes on Earth (Rohde et al., 2008).

This study examines Late Holocene CH_4 records with centimetre-scale resolution from five polar ice cores with contrasting site characteristics (Table 1). Four of the cores are from Greenland and one is from East Antarctica (Fig. S1). Accumulation rate and temperature, the principal factors affecting firn densification rates, vary considerably between the different cores. Concentrations of chemical impurities contained within the ice can also vary by an order of magnitude (Table 1). Here we compare the ultra-high resolution CH_4 records of the five different ice cores to show that the high frequency non-atmospheric signals we previously observed in NEEM-2011-S1 ice are not unique to this site. Furthermore, we demonstrate how several site characteristics influence the frequency and magnitude of non-atmospheric signals.

2   Methods

2.1   Sample description

The ice core samples analysed in this study are listed in Table 1. Archived samples were obtained from NEEM, D4 and North Greenland Ice Core Project (NGRIP). The NEEM section was chosen to extend the existing NEEM-2011-S1 record further back in time. The D4 record extends the NEEM-2011-S1 record forward in time and is from a warmer Greenland site with twice the accumulation rate. The NGRIP samples are from two Late Holocene depth intervals. A new ice core was retrieved from Tunu, NE Greenland, where accumulation rates are about half those of NEEM or NGRIP. Hereafter the Tunu core will be referred to as Tunu13 to avoid confusion with previous drilling projects. Two Tunu13 cores were drilled: the first (Tunu13 Main) extended from the surface to 214 m depth and the second (Tunu13 B) from the surface to 140 m depth. The online gas and chemistry records used in this study are predominantly from the Tunu13 Main core with sections of Tunu13 B spliced in where poor core quality of Tunu13 Main core caused deterioration of the records (Table S1). Prior to analysis, the Tunu13 cores were logged at the National Ice Core Laboratory. Bottom depths of bubble-free layers were recorded and top depths were recorded if the layer's width exceeded 4 mm. It was not possible to discriminate visually between bubble-free layers that were melt layers and those that were wind crusts (fine-grained, sintered layers thought to result from wind action (Alley, 1988)). Both are likely to occur as Tunu is a windy site and our field team found melt layers from the 2012 Greenland melt event. The B40 ice core was drilled close to Kohnen Station, Dronning Maud Land, E Antarctica, by the Alfred Wegner Institute and represents the coldest site with lowest impurity loading of the cores featured in this study (Table 1).

2.2   Analytical methods

All the ice cores listed in Table 1 were analysed at the Desert Research Institute, Reno NV, USA, using a continuous ice core melter system with online gas measurements (Rhodes et al., 2015, 2013). Chemical concentrations in the liquid were measured simultaneously, as described previously (McConnell et al., 2007, 2002).

An optical feedback cavity enhanced absorption spectrometer (SARA, developed at Laboratoire Interdisciplinaire de Physique, University Grenoble Alpes, Grenoble, France) (Morville et al., 2005) was used to analyse methane—the same instrument as used by Rhodes et al. (2013) and Faïn et al. (2014). The system response time (time to reach 90% of concentration step change (t90)) was 109 seconds, equivalent to 9.4–12.3 cm, depending on the melt rate used for each ice core (Table S1). Methane data were corrected for dissolution in the melted ice core sample following methods described previously (Rhodes et al., 2013). Some system parameters, such as melt rate, varied between ice cores to ensure the best compromise between measurement efficiency and resolution (mainly in liquid phase) and different solubility corrections are used to account for this (Table S1). Allan variance tests performed on measurements of synthetic sample (standard gas mixed with degassed water) suggested an optimal integration time > 1000 s. However, to maximise depth resolution we used an integration time of 5 s, for which Allan variance tests suggest an internal precision of 1.7 ppb (2 σ).

To limit entry of ambient air into the analytical system as breaks in the core were encountered, ice was removed at any angled breaks to obtain a planar surface on which the next ice stick could sit squarely. This resulted in some short sections of data loss. Methane data were manually screened for spikes resulting from ambient air entry at the melterhead (see also Sect. 3.2) because an automated screening algorithm proved too aggressive, resulting in the removal of real variability, as confirmed by discrete CH_4 measurements.

Methane and chemistry data were mapped onto a depth scale using high resolution (0.1–0.5 Hz acquisition rate) liquid conductivity data and time-depth relationships recorded by system operators. A constant melt rate for each metre length of core is assumed. Depth scale uncertainties are estimated to be ± 2 cm (2 σ). The ice and gas age scales used for each ice core are listed in Table 1.

For comparison, discrete samples from the Tunu13 ice core were analysed at Oregon State University for methane concentration and total air content. Minor adjustments to the methods of Mitchell et al. (2011) are described in the Supplementary Material. Twenty-four ~15 cm depth sections were analysed at 6 cm resolution. External precision

1 of these data, estimated as pooled standard deviation of 34 duplicate (horizontally-
2 adjacent) sample sets, is 3.1 ppb for CH_4 and 0.002 cm^3 STP g^{-1} ice for total air content (1
3 σ).

2.3   Firn air transport models

5 We compare our empirical data to theoretical model predictions of CH_4 concentrations in
6 closed bubbles resulting from layered gas trapping produced by the Center for Ice and
7 Climate (CIC), Copenhagen, firn air transport model (Buizert et al., 2012). This model
8 includes parameterisation of stochastic gas trapping related to local density variability
9 (Mitchell et al., 2015). All experiments are run for the WAIS Divide ice core site
10 because high resolution local density data are available, as well as firn air sample data
11 needed to calibrate the diffusivity profile in the open pores. Model simulations are
12 performed at 1 cm vertical resolution to accurately capture the influence of layered
13 bubble trapping. Further details on modeling centimetre-scale air occlusion are provided
14 by Mitchell at al. (2015). The model simulations for the WAIS Divide ice core site can
15 be compared to Greenland ice core sites because the site conditions, particularly
16 temperature and accumulation rate, the principal factors to influence densification are
17 relatively similar (Table 1).

18 In addition, we use the Oregon State University (OSU) firn air transport model (Buizert et
19 al., 2012), adapted for palaeo-applications (Rosen et al., 2014), to estimate the smoothing
20 effect that diffusion in the firn has on the CH_4 atmospheric history at each ice core site
21 (Fig. S2).

22

3   Results and discussion

3.1   Integrity of the atmospheric CH_4 history from ice cores

25 Multi-decadal scale atmospheric CH_4 variability, previously observed in Law Dome DSS
26 (MacFarling Meure et al., 2006), WAIS Divide (Mitchell et al., 2011), GISP2 (Mitchell et
27 al., 2013) and NEEM-2011-S1 (Rhodes et al., 2013), is faithfully replicated in all the ice
28 cores analysed in this study (Fig. 2). The multi-decadal signals recorded in each core
29 vary in amplitude because the original atmospheric signal has been smoothed to a

1   different extent at each site by firn-based processes (diffusive mixing and gradual bubble

2   occlusion). As expected, the low accumulation, cold, East Antarctic core B40 exhibits

3   the most extreme firn-based smoothing (orange line), and the Tunu13 record (green line)

4   shows significant signal damping compared to NGRIP (purple line) due to the lower

5   accumulation rates at Tunu. The estimated gas age distribution width (full width at half

6   maximum) at close-off depth for present-day conditions at each ice core site ranges from

7   14 yr at D4 to 65 yr at B40 (Table 1). Atmospheric signals of a shorter period than the

8   gas age distribution width are unlikely to be resolved with their full amplitude in the ice

9   core record.

10   **3.2   Potential in-situ CH_4 production and melt layers**

11   The continuous CH_4 records of all the ice cores analysed contained a high frequency

12   component superimposed on the coherent atmospheric signals shown in figure 2. For this

13   study it was particularly challenging to confidently distinguish between isolated

14   anomalously high CH_4 spikes present in-situ and those resulting from contamination by

15   ambient air. Forest fire haze over Reno during the analytical campaign meant that it was

16   not possible to rely on the absence of a carbon monoxide (CO) signal as indicative of

17   ambient air entry, as has previously been the case (Rhodes et al., 2013). This problem

18   was compounded by poor core quality (high break density, Table S1) in some core

19   sections. However, in a limited number of cases, discussed below, we were able to

20   distinguish between ambient air contamination and in-situ CH_4 signals.

21   Discrete CH_4 measurements performed on Tunu13 ice provided useful information

22   concerning isolated in-situ CH_4 spikes. The CH_4 concentrations of 5 of the 146 discrete

23   samples analysed (Table 2) were anomalously high, between 15 and 80 ppb greater than

24   adjacent samples. The elevated CH_4 samples also had relatively low air content values of

25   0.0847–0.0970 cm^3 STP/g ice compared to median of 0.1002 cm STP/g ice (Table 2),

26   negating the possibility of sample contamination by an ambient air leak during analysis.

27   The five anomalous samples were all located within 2.5 cm of bubble-free layers logged

28   during processing (Figs. 3A, 3F-H, Table S2). We therefore hypothesize that these

29   bubble-free layers are melt layers. Anomalously high CH_4 values in ice cores have been

30   linked to melt layers because a) the solubility of CH_4 in water is greater than that of bulk

1   air, and/or b) previous studies suggest a potential for CH_4 production by microbial

2   activity, via reaction pathways that are currently unknown (Campen et al., 2003; NEEM

3   community members, 2013).

4   The CH_4 concentration and air content of each of these discrete samples represent a

5   mixture of air from standard bubbly ice and air from a melt layer. Each discrete sample

6   typically spanned 6 cm of ice core depth and, by comparison, the melt layers in the

7   Tunu13 cores were very thin, typically spanning < 5 mm depth. Given that we know the

8   dimensions of each sample and the proportion of the sample volume occupied by the melt

9   layer, we can estimate the CH_4 concentration in the melt layer itself (Table 2). We

10   assume that the air content of each melt layer is 0.0095 ± 0.0037 cm^3 STP g^{-1} ice (1 σ

11   uncertainty, n = 12), which is the value measured at Oregon State University on melt

12   layer samples (from the 2012 melt event) collected at Summit, Greenland. Estimated

13   melt layer CH_4 concentrations range from 1829 (+704/-310) ppb to 6355 (+3585/-1574)

14   ppb, equivalent to 2.5–8.6 fold the atmospheric CH_4 concentrations at the time of melt

15   layer formation (Table 2). We then calculate the predicted CH_4 concentration of the melt

16   layers if dissolution of CH_4 from the atmosphere in liquid water reached equilibrium

17   (Table 2). Methane becomes relatively enriched in liquid water that is in equilibrium

18   with the atmosphere because methane is more soluble than nitrogen (Sander, 2015). The

19   predicted equilibrium CH_4 concentrations are all significantly lower than our estimated

20   melt layer concentrations, suggesting that another process, in addition to dissolution,

21   must contribute to the enrichment of CH_4 in melt layers. Our findings therefore support

22   those of the NEEM Community Members (2013), who found elevated CH_4

23   concentrations in excess of Henry's Law predictions across a melt layer in the Dye-3

24   (Greenland) ice core, and also those of Campen et al. (2003), who measured anomalously

25   high CH_4 values that could not be explained by dissolution effects alone. We note that in

26   this study we had to infer the CH_4 concentration of the melt layer because we were not

27   able to obtain a sample of pure melt layer, and the CH_4 values we estimate are relatively

28   uncertain.

29   In light of this apparent link between anomalously high CH_4 concentrations and melt

30   layers in Tunu13 ice, we re-examined the continuous CH_4 data and identified a further 14

bubble-free layers, coincident in depth with anomalous CH_4 spikes, that we assume are melt layers (Table S2). The onset of these events can be extremely abrupt, making them appear similar to ambient air contamination. 12 bubble-free layer depths had no continuous CH_4 data, usually because data had been removed due to mixing with standard at start/end of a run or because the ice had been removed across a badly-shaped break. The CH_4 record at a further 20 bubble-free layer depths was affected by ambient air contamination. There are also 78 bubble-free layer depths for which the CH_4 record appears anomaly-free, suggesting that many of these observed bubble-free layers could be wind crusts, not melt layers (Orsi et al., 2015). Alternatively, many of these bubble-free layers did not span the entire horizontal area of the 10 cm diameter core and may have not have been included in the 3.4 x 3.4 cm melter stick cut from the core.

We investigated the chemical composition (nitrate, refractory black carbon and ammonium concentrations) of the suspected-melt layers with anomalously high CH_4, because these chemical species were associated with isolated CH_4 spikes in the NEEM-S1-2011 ice core (Rhodes et al., 2013) and GISP2 ice core ((Mitchell et al., 2013) ammonium only). In the Tunu13 record, there was no significant difference between chemical concentrations at depths coincident with anomalously high CH_4 linked to melt layers and chemical concentrations at other depths (Fig. S3).

3.3 Lock-in-zone CH_4 variability

Methane concentrations were measured continuously up-core into the lock-in zone for three ice cores: D4, Tunu13 and B40. We observed a marked increase in the amplitude of decimetre-scale variability and a gradual decrease in gas flow to the instrument through the lock-in zone (Fig. S4), similar to results produced by continuous CH_4 analysis of the lock-in zones in NEEM-2011-S1 (Rhodes et al., 2013) and WAIS Divide (WDC05A, Mitchell et al. (2015)) ice cores. The sharp increase in the amplitude of high frequency variability by up to 10-fold makes the base of the lock-in zone (close-off depth) easily recognisable in continuous CH_4 data. We estimate the close-off depth to be 82 m at D4, 73 m at Tunu13 and 95 m at B40, comparable to values from firn air field campaigns at the latter two sites (Tunu13: Butler et al., 1999; B40: Weiler, 2008). The D4 continuous CH_4 data appear to encompass the entire lock-in zone.

1   Initial examination suggests that the magnitude of lock-in zone CH_4 variability varies

2   significantly between cores (Fig. S4) but it is not possible to quantify the degree of

3   ambient air contamination influencing our lock-in zone measurements, either from

4   laboratory air (~1890 ppb) via inter-connected open porosity or from post-coring bubble

5   closure (Aydin et al., 2010). It is therefore difficult to quantify the influence of layered

6   bubble trapping on lock-in zone CH_4 variability. However, we have reason to believe

7   that the proportion of ambient laboratory air versus air from the closed porosity may be

8   low because continuous CH_4 measurements of WAIS Divide lock-in zone samples

9   conducted using the same analytical system were well replicated by discrete CH_4

10 measurements (see Mitchell et al. (2015) Fig. S5). Furthermore, Mitchell et al. (2015)

11 used $\delta^{15}N$ of N_2 data measured on the WAIS Divide lock-in zone samples to calculate the

12 proportion of air affected by post-coring bubble closure as $10.6 \pm 6.1\%$; this value should

13 be considered as an upper estimate as the core used in that study was stored for ~ 6 yr

14 prior to analysis.

15 **3.4   High frequency non-atmospheric signals in mature ice**

16 **3.4.1   Observations**

17 In the mature ice phase below the close-off depth we observe significant decimetre-scale

18 variability in the CH_4 records of every ice core analysed. In each case, it is impossible

19 that this high frequency signal could have existed in the atmosphere at the ice sheet

20 surface and survived the low-pass filter action of the firn—the gas age distribution widths

21 (Table 1) are greater than the approximate signal periods. We initially focus in detail on

22 only Tunu13 and B40 because these are the most complete records, with relatively little

23 ice removed prior to analysis and few ambient air entry problems, both factors linked to

24 the number of core breaks (Table S1).

25 A smoothing spline is subtracted from the CH_4 record of each site to effectively remove

26 the atmospheric signal (Fig. 3A&B, Tunu13 shown). The residual CH_4 record contains a

27 high frequency, non-atmospheric signal and analytical noise (Fig. 3B). The mean peak-

28 to-peak amplitude (see Supplementary Material) of the residual high frequency CH_4 in

29 the Tunu13 record from 987 to 1870 AD gas age is 5.3 ppb (median is 3.7 ppb) and

30 varies between 2 ppb and 42 ppb. Variability of similar peak-to-peak amplitude and

frequency observed along the NEEM ice core continuous CH_4 profile was attributed to analytical system noise (Chappellaz et al., 2013). Here, we have confidence that we capture a high frequency signal present above the analytical noise in some sections of the record because discrete CH_4 measurements on the Tunu13 core conducted at 6 cm resolution also show substantial variability within each 15 cm depth section. CH_4 concentrations in adjacent samples differ by up to 32 ppb, but more typically by 3.4 ppb, and reproduce some of the decimetre-scale changes resolved by the continuous measurements (Fig. 3C-E). CH_4 oscillations captured by the discrete measurements are larger in amplitude than those in the continuous gas record because the continuous gas analysis system causes more signal smoothing that the discrete analysis (Stowasser et al., 2012) (Table S1, Fig S2). The 5.3 ppb mean peak-to-peak amplitude of this high frequency non-atmospheric signal must therefore be a minimum estimate of the true signal in the ice.

A high frequency, non-atmospheric signal in excess of analytical noise is also present in sections of the B40 continuous CH_4 record and it is reproducible; we measured replicate ice core sticks on different days and were able to resolve very similar decimeter-scale features in ice samples from 114–120 m depth (Fig. 4). The sharp CH_4 troughs at 122.8, 122.6, 122.3, 121.3 and 120.2 m are particularly well replicated and highly unlikely to be analytical artifacts. The mean peak-to-peak amplitude of the high frequency non-atmospheric signal in this section of the B40 record is 5.4 ppb (median is 5.1 ppb).

3.4.2 Evidence for layered bubble trapping

Our results demonstrate that the quasi-annual variability previously observed in the ice phase of the NEEM-2011-S1 core (Rhodes et al., 2013) is not unique to NEEM or to Greenlandic ice. The question now is: what causes it? If it is an artifact of layered bubble trapping, as speculated for NEEM-2011-S1, the observed decimetre-scale variability should respond in a predictable way to several factors that vary over time and between ice core sites. We therefore systematically examine our empirical data to assess the influence of each factor and judge whether any relationship is consistent with the mechanism of layered bubble trapping.

- Atmospheric CH_4 growth rate

1 Our conceptual model of layered bubble trapping predicts that the difference in CH_4

2 concentration between adjacent layers (ΔCH_4) should increase with the CH_4 concentration

3 gradient in the firn column, which is dictated by the atmospheric CH_4 growth rate (Fig.

4 1). We can clearly observe this relationship in the Tunu13 record; amplitudes of the

5 decimetre-scale CH_4 oscillations are greatest when the atmospheric CH_4 concentration

6 shows a sustained trend of increase or decrease, particularly during the steep post-

7 Industrial Revolution CH_4 rise and the growth and decay in atmospheric CH_4

8 concentrations associated with the prominent CH_4 oscillation centered on 1550 AD (Fig.

9 3B).

10 To explore this relationship quantitatively, we compare the CH_4 growth rate to the

11 standard deviation (σ) of the high frequency CH_4 residual (data minus spline, as Fig. 3B)

12 for moving windowed sections of the Tunu13 record. Windows are 40 yr in length and

13 are calculated every 10 yr interval. Strong linear relationships between CH_4 growth rate

14 and the magnitude of high frequency variability are revealed for atmospheric CH_4 growth

15 and decay rates > 0.4 ppb yr^{-1} (Fig. 5E). The gradients of the linear relationships are

16 similar in both cases (7–8 ppb σ-CH_4 /ppb yr^{-1} growth rate). At low growth rates (< 0.4

17 ppb yr^{-1}) σ-CH_4 values reflect the analytical precision of 1.7 ppb. The observation that σ-

18 CH_4 only increases beyond analytical noise at growth rate > 0.4 ppb yr^{-1} heavily

19 implicates the mechanism of layered bubble trapping as the cause of the high frequency

20 CH_4 signal because it requires sustained trend of change in atmospheric concentration to

21 produce CH_4 artifacts (Fig. 1). We therefore define high frequency non-atmospheric CH_4

22 variability in excess of analytical noise as "trapping signal".

23 This analysis was repeated on the high frequency CH_4 residual records from other ice

24 cores: B40, NEEM-2011-S1, D4 and NGRIP (Fig. 5 A-D). For NGRIP, only data from

25 1050–1240 AD and 1774–1860 AD (gas age) were used, the latter with a 10 yr length

26 window to avoid data gaps. For NEEM-2011-S1, data from 1450–1840 AD were used.

27 Any 40 yr time window with a data gap > 5 yr duration was discarded from analysis. We

28 note that the CH_4 growth rate recorded in the ice core is not strictly equivalent to the

29 atmospheric growth rate because firn-based smoothing may have caused some damping

30 of the signal (Fig. 2). The B40 record is significantly affected by firn-based smoothing

31 (Fig. S2), which reduces the growth rate captured by the ice core archive. The B40

1   record is also severely impacted by system-based smoothing (Fig. S2), which damps the

2   trapping signal to within range of the analytical noise for much of the record, excepting

3   the section displayed in figure 4. The combination of these two effects destroys any

4   relationship between atmospheric growth rate and amplitude of the high frequency signal

5   (Fig. 5A). There is also little sign of a relationship between growth rate and σ-CH_4 in the

6   NEEM-2011-S1 data (Fig. 5B) and we speculate this is the result of a more aggressive

7   ambient air screening method applied by Rhodes et al. (2013) that may have removed real

8   variability.

9   Results are more encouraging for D4 and NGRIP as both sites exhibit linear relationships

10   between CH_4 growth rate and the trapping signal magnitude (Fig. 5C&D). Both negative

11   and positive growth rates at NGRIP exhibit the same gradient of change with σ-CH_4. The

12   consistency of results between sites is important for the identification of layered bubble

13   trapping as the mechanism behind the high frequency variability. Further support can be

14   drawn from the CIC firn air transport model, which predicts a linear relationship between

15   atmospheric growth rate and the CH_4 trapping signal magnitude at WAIS Divide (red

16   line, Fig. 5F). When the Tunu13, D4 and NGRIP data are all plotted on the same axes

17   with the WAIS Divide model simulation (Fig. 5F), the gradient of the modeled linear

18   relationship is within the range of gradients of our empirical data from 3 different

19   Greenland ice core sites. Clearly, the CH_4 trapping signal magnitude (σ-CH_4) does not

20   have the same sensitivity to growth rate at all ice core sites; another factor is influencing

21   CH_4 variability, as we explore below.

22   For completeness we note that physics tells us that there can still be a tiny layered bubble

23   trapping signal at zero growth rate due to the effect of gravity. As CH_4 is lighter than air,

24   gravity reduces the CH_4 concentration with depth relative to the concentration in the

25   atmosphere. Thus at zero growth rate there is still a CH_4 gradient in the firn that can

26   result in the generation of a trapping signal via layered gas occlusion. This also means

27   that at positive atmospheric growth rates, the gravitational gradient must be overcome in

28   order to generate CH_4 oscillations related to layering. This is why the modeled WAIS

29   Divide growth rate vs. σ-CH_4 plot intersects the x-axis at a slightly positive growth rate

30   and σ-CH_4 is predicted to be 0.11 ppb at zero growth rate (Fig. 5F). This effect is an

31   order of magnitude smaller than the analytical noise and is not detectable.

1   *- Accumulation rate*

2   At a constant atmospheric growth rate, the CH_4 trapping signal amplitude produced by

3   layered bubble trapping should be determined by the difference in age between the air

4   trapped relatively early compared to younger air trapped relatively late (t_2 minus t_1 on

5   Fig. 1).   One factor that will affect how quickly an adjacent layer is closed off is

6   accumulation rate (A)—more new snow accumulation will cause layers to spend less time

7   in the firn column reducing the time interval over which layered bubble trapping can

8   occur.   We test this hypothesis by comparing the CH_4 trapping signal magnitude in ice

9   cores with different accumulation rates (Fig. 6A&B).   Comparison is performed for two

10   discrete time periods (gas age) for which we have good quality (continuous and above

11   analytical noise) CH_4 residual data from three cores, and we assume all three sites

12   experienced the same atmospheric growth rate.   As expected, there is a significant

13   decrease in σ-CH_4 with increasing accumulation rate for the 1770–1900 AD time period

14   (Fig. 7B), but the 1490–1630 AD interval shows shows no trend (Fig. 6A).

15   However, if we adjust the σ-CH_4 values of each ice core to compensate for the

16   differences in the smoothing effect of the analytical system, the results from the two time

17   intervals become more consistent (Fig. 6C&D).   To perform this adjustment, we assume

18   that the high frequency signal has an annual periodicity and consult the Bode plots

19   generated from switching the analytical system between two gas standards, to determine

20   what fraction of the original amplitude is retained by the system (Fig. S2).   The nature of

21   this relationship differs between time slices considered.   An inverse relationship between

22   σ-CH_4 and annual layer thickness is identifiable for the 1490–1630 AD interval and a

23   power law fit is applied, but a linear relationship would also be applicable here.   A power

24   law relationship is identifiable between annual layer thickness and σ-CH_4 for the 1770–

25   1900 AD time period, which has the greatest range of annual layer thickness and σ-CH_4

26   values.   These corrected data suggest that, at a fixed growth rate, an inverse relationship

27   exists between accumulation rate and the magnitude of CH_4 variability (σ-CH_4).   This is

28   how we would expect CH_4 trapping signal to respond to accumulation rate.

29   CIC firn air transport model simulations for WAIS Divide exhibit a similar power law

30   relationship to the empirical data, whereby σ-CH_4 is proportional to $1/A^{1.47}$.   The slope is

1   the result of two separate effects. First, increasing A decreases the time adjacent layers

2   spend in the firn column, which by itself should cause CH_4 trapping signal to scale as

3     $1/A$. Second, at increased A the advective gas transport in the open pores is enhanced,

4   and this reduces the CH_4 gradient down the firn column. If bubbles are then trapped over

5   the same depth range, the amplitude of CH_4 variability will be reduced, and this effect

6   appears to scale as $1/A^{0.47}$ in the firn model. An important caveat is that the model

7   assumes no change in the firn density profile with changing accumulation rate, which is

8   unrealistic. However, the model does appear to capture a response of CH_4 trapping signal

9   to accumulation rate that is roughly comparable to that observable in the real-world data.

10   *- Firn layering*

11   Another factor that should influence the amount of time that passes between early and

12   late bubble closure is the degree of contrast between the physical properties of firn in

13   adjacent layers. There is no doubt that the physical properties of firn ultimately control

14   when a bubble is occluded, or a layer is completely sealed off. The relative importance

15   of local density variability, firn microstructure, permeability and/or porosity in this

16   process is actively debated. The traditional interpretation of density as the principal

17   influence on bubble occlusion is being challenged (Gregory et al., 2014). However, we

18   concentrate on the potential influence of local density variability in this section.

19   The controls on density layering in the firn are poorly understood, but a recent study

20   suggests that variability near the firn-ice transition is higher at warmer, high

21   accumulation sites (Hörhold et al., 2011). It is difficult to test the effects of density

22   layering because we do not have the high resolution density information required to do

23   so. However, we can use the CIC firn air transport model, which utilises high resolution

24   density data for the WAIS Divide ice core, to make a prediction. In these simulations, we

25   define the density layering to be $\rho_{layer} = \rho - <\rho>$ with the local firn densities (ρ) as given

26   by the high resolution measurements, and the bulk density ($<\rho>$) as given by a spline fit

27   to those data. We then run the model several times with a density profile that equals $\rho =$

28     $<\rho> + \alpha\rho_{layer}$. By varying the scaling parameter α between 0 and 1.6 we can effectively

29   control the magnitude of the firn density layering. As we would expect, no high

30   frequency CH_4 trapping signal is produced in the absence of density layering ($\alpha = 0$) (Fig.

S5). When the magnitudes of the local density anomalies are halved ($\alpha = 0.5$), the trapping signal amplitude decreases slightly more than 2-fold from 7.3 ppb to 3.2 ppb. This effect is minor compared to that of accumulation rate or atmospheric growth rate. However, it may explain why interior Antarctic sites, like B40, which have less pronounced seasonality in density at the firn-ice transition compared to coastal Antarctic or Greenland locations (Hörhold et al., 2011) may show only a moderate trapping signal despite the extremely low accumulation rates.

3.5 Layered gas trapping mechanism

3.5.1 Spatial and temporal information

Having established that the high frequency CH_4 signal we observe in all the ice cores in this study shows characteristics consistent with the mechanism of layered gas trapping (Fig. 1), we are able to discern aspects of this physical process.

First, the CH_4 trapping signal measured for the different ice core sites allows us to estimate the age difference between the air samples trapped in adjacent layers (t_2 minus t_1 on Fig. 1). High frequency CH_4 residual data, corrected for system smoothing effects (Sect. 3.4.2) from the 1810–1860 AD time interval, which has an atmospheric growth rate of 1.5 ppb yr^{-1} (in D4—the least susceptible record to firn-based smoothing of the atmospheric signal), suggest a gas age difference between adjacent layers of 23 yr at Tunu13, 2.4 yr at D4 and 5 yr at NGRIP. These values can be compared to previously published estimates of 10 yr for WAIS Divide (Mitchell et al., 2015), 12 yr for NEEM-2011-S1 (Rhodes et al., 2013) and 2 yr for Law Dome (Etheridge et al., 1992). Unsurprisingly, the gas age difference between adjacent layers is greater at lower accumulation sites. To negate the issue of smoothing associated with the analytical system, we also consider Tunu13 discrete measurements, which show a maximum oscillation of 32 ppb amplitude at an atmospheric growth rate of 1.5 ppb yr^{-1} (Fig. 3C). The age difference between layers in this case would be 21 yr, which is very close to the estimate above.

Second, the frequency of CH_4 oscillations resulting from layered bubble trapping should reflect the difference in depth, and therefore also ice age (not the age of the gas trapped inside the bubbles, as discussed above) between adjacent firn layers where bubbles are

18

1   closed off at different times. To test this with our ice core data we perform multi-taper

2   method (MTM) spectral analysis of the Tunu13, D4, NGRIP and B40 CH_4 records (Fig.

3   7). Spectral analysis is performed in the ice age domain because we believe that physical

4   properties of the firn/ice are ultimately responsible for the high frequency artifacts

5   recorded in the gas phase at the same depth. Prior to analysis, the data in each 40 yr

6   window (as Sect. 3.4.2) are interpolated to an even ice age spacing that is twice the

7   median sample spacing and any windows containing data gaps > 2 yr are ignored. We

8   then average the MTM spectra produced to generate mean spectra for sections of the

9   record with relatively high or low growth rate, or in the case of D4, sections of the record

10   encompassing only mature ice or some firn.

11   Sections of the Tunu13 record with CH_4 growth rates > 0.4 ppb yr^{-1} exhibit spectral peaks

12   at 1 yr period in the ice age domain and the averaged spectrum for growth rates > 0.4 ppb

13   yr^{-1} has a significant 1 yr periodicity (95% confidence) (Fig. 7). By contrast, sections of

14   the Tunu13 record with growth rates < ± 0.4 ppb yr^{-1} show no significant periodicity.

15   The high accumulation Greenland ice core D4 shows an annual periodicity in CH_4, but it

16   only becomes significant when data from the lock-in zone are included (Fig. 7). NGRIP

17   shows small spectral peaks at 1 yr period for 2 out of 4 time windows with growth rates >

18   0.2 ppb yr^{-1} but the peak in the averaged spectrum is not significant (Fig. 7). Again,

19   NGRIP data sections with growth rates < 0.2 ppb yr^{-1} exhibit no periodicity. No

20   significant periodicity is resolved in the B40 high frequency residual CH_4 record,

21   potentially because any annual signal has been removed by analytical system smoothing.

22   The significant annual periodicity resolved in the Tunu13 and D4 records during periods

23   of relatively high growth rates strongly suggests that the mechanism of layered bubble

24   trapping is linked to regular, seasonal variations in the physical properties of the firn

25   pack, over a wide range of Greenland ice core site conditions. The quasi-annual high

26   frequency signal observed in mature NEEM-2011-S1 ice (Rhodes et al., 2013) could also

27   be added to this list. We note that even if there is some ambient air contamination of D4

28   lock-in zone CH_4 measurements, the wavelength of the CH_4 oscillations in the lock-in

29   zone should reflect the depth spacing of alternating layers with contrasting ratios of open

30   to closed porosity, and therefore relatively more or less contamination (Fig. 7).

3.5.2 Implications for bubble closure in the firn column

The regular oscillations between relatively young and relatively old air trapped in the ice core air bubbles suggest that the early-closure layers (p_h on Fig. 1) are not sealing layers which prevent vertical diffusion. In other words, some degree of open porosity/permeability must be maintained in these early-closure layers to allow relatively young air to diffuse down through the firn pack towards the late-closure layers (p_l on Fig. 1). This movement could be via vertical cracks or channels of open porosity tracking around isolated clusters of closed pores in the early-closure layers (Keegan et al., 2014). Furthermore, our results suggest that this situation must be maintained for upwards of 20 yr at the Tunu13 site.

The onset of the lock-in or non-diffusive zone (Sowers et al., 1992) is commonly believed to be linked to horizontally-expansive sealing layers. Field measurements of firn air (air pumped from the open porosity in the firn) provide strong evidence for such sealing layers by demonstrating a lack of vertical mixing within the lock-in zone. For example, halocarbon tracers linked to anthropogenic industrial activity are effectively absent in the lock-in zone firn air at many sites (Butler et al., 1999; Severinghaus et al., 2010; Sturrock et al., 2002). To first order, the trapping signal we observe in the ice cores therefore suggests that significant bubble closure in the early-closure layers must occur above the lock-in depth, where vertical diffusion of the relatively young air required to form the regular CH_4 oscillations is not impeded. However, we do not rule out a contribution to the trapping signal from within the lock-in zone because a) some vertical pore connectivity in the lock-in zone is required to explain firn air observations at NEEM (Buizert et al., 2012) and b) air content of mature ice is not consistent with fully sealing layers at the lock-in depth (Martinerie et al., 1992). Measurements of WAIS Divide lock-in zone samples suggest that much of the trapping signal is inherited from bubble trapping above the lock-in depth, below which the signal gradually becomes muted as vertical gas mixing is limited (Mitchell et al., 2015).

Our results suggest that the variations in local density and/or other related physical properties, such as open porosity or grain size (Gregory et al., 2014) maintain an imprint of annual variability towards the base of the firn column that is strong enough to produce

1 regular layering in the firn, resulting in a CH_4 trapping signal with a significant annual

2 periodicity. It is still not clear precisely how and why layering in polar firn evolves with

3 depth and time in the way that it does. Hörhold et al. (2012) suggested that "impurities"

4 which exhibit an annual cycle in concentration may act to promote densification by

5 softening the impurity-rich winter firn layers. Hörhold et al. (2012) reported positive

6 correlations between soluble calcium (Ca^{2+}) concentration and local density but their

7 choice of Ca^{2+} was not supported by any causal physical link between Ca^{2+} and

8 densification rate. Ensuing work suggested that chloride (Cl^-) and fluoride (F^-) were

9 more likely candidates to drive densification at NEEM (Fujita et al., 2014), drawing on

10 early experiments which detail how substitution of Cl^- and F^- ions into the ice lattice

11 promotes dislocations and causes a softening effect (Jones, 1967; Nakamura and Jones,

12 1970). A subsequent study confirms these ideas by demonstrating their application to the

13 Dome Fuji ice core (Fujita et al., 2016). It is important to note that Fujita et al. (2016,

14 2014) also invoke a second, independent process that contributes to densification which

15 involves textural effects and is related to depositional conditions.

16 Our data cannot resolve this issue, but we can use the chemical concentrations measured

17 as a proxy for local density, assuming that winter/spring chemical species like Ca and Cl

18 are enriched in the relatively dense layers. In the Tunu13 ice core, concentrations of Ca

19 and Cl show significant negative correlation ($p < 0.05$) with CH_4 anomalies when growth

20 rates are positive (Fig. 8). A similar relationship is observable for the short section of the

21 B40 core with significant CH_4 trapping signal, using Na in place of Cl in this instance

22 because it is easier to measure at very low concentrations (Fig. 4B). These observations

23 confirm the seasonality of layered gas trapping that we have assumed—Ca and Cl-rich,

24 dense, layers trap air earlier, preserving a relatively low CH_4 concentration when

25 atmospheric CH_4 is increasing, and vice versa. Correlation between impurity levels in the

26 ice and CH_4 anomalies does not signify a causal link between them. It makes sense that

27 the correlation between ice chemistry and CH_4 is stronger at high growth rates because

28 the trapping signal produced at these times has relatively a high amplitude and an annual

29 periodicity. What is more interesting is that the sign of the correlation coefficient

30 between Ca or Cl and the high frequency CH_4 signal switches when CH_4 growth rate is

31 negative rather than positive (Fig. 8). When atmospheric CH_4 is decreasing, a Ca-Cl-rich

1 layer that closes off early will trap air with a relatively high CH_4 concentration. This is

2 an important final piece of evidence to attribute the high frequency CH_4 signal in ice

3 cores to layered bubble trapping.

4

4 Summary

4.1 Methane artifacts related to melt layers

7 We have demonstrated that narrow, isolated peaks in CH_4 concentration in the Tunu13 ice

8 core record are located at depths coincident with bubble-free layers assumed to be melt

9 layers. CH_4 measurements on discrete ice samples enabled us to confidently link melt

10 layers and CH_4 enrichment, circumventing the complication of potential ambient air

11 contamination from the continuous-flow system. These findings contrast with our

12 previous study (Rhodes et al., 2013), in which we found no melt layers associated with

13 anomalous CH_4 signals in the NEEM-2011-S1 core, but are in agreement with published

14 data showing trace gas enrichment across melt layers in the Dye 3 (Greenland) ice core

15 (NEEM community members, 2013; Neftel et al., 1983). Furthermore, we confirm this

16 and earlier work (Campen et al., 2003; NEEM community members, 2013) suggesting

17 that dissolution of CH_4 in the liquid phase cannot account for the full magnitude of CH_4

18 enrichment in melt layers, suggesting, but not proving, that biological activity may be in

19 part responsible for the observed CH_4 enrichment. Additionally, we find no significant

20 relationships between the anomalously high CH_4 levels at melt layer depths and

21 concentrations of chemical species (NH_4^+, rBC or NO_3^-) present in the ice phase of the

22 Tunu13 ice core.

23 In the absence of a systematic, reliable methodology to confidently distinguish between

24 elevated in-situ CH_4 signals and ambient air contamination, this study can only contribute

25 limited information regarding the potential for biological in-situ production of methane in

26 polar ice. The implications of biological in-situ production in polar ice are so far-

27 reaching (Priscu and Hand, 2010) that it deserves further investigation by a dedicated

28 multi-disciplinary project. Continuous trace gas analysis is an effective tool for screening

29 cores to identify depth ranges with interesting signals but further analysis including

30 $\delta^{13}CH_4$, organic species and meticulous microbiological characterisation are needed.

4.2 Methane artifacts resulting from layered bubble trapping

This study uses high resolution continuous CH_4 data from five Late Holocene ice cores to demonstrate that layered bubble trapping causes high frequency (decimetre-scale) oscillations in the CH_4 record of mature ice from both Antarctica and Greenland when there is a sustained positive or negative trend in atmospheric growth rate. This trapping signal has been reproduced by discrete and continuous CH_4 measurements and cannot reflect atmospheric history because firn-based smoothing processes would have removed it.

Using empirical data supported by firn air transport model simulations we demonstrate that the CH_4 trapping signal responds in predictable ways to atmospheric growth rate and site specific factors, particularly accumulation rate. The amplitude of the CH_4 trapping signal increases with atmospheric growth rate and seasonal density contrasts, and decreases with accumulation rate. The layered bubble trapping signal in two Greenland ice core records has a significant annual periodicity, demonstrating that the seasonal contrasts in firn physical properties which develop above the firn-ice transition are regular and uniform enough to generate periodic CH_4 artifacts.

5 Implications

5.1 Implications for future ice core trace gas analysis

- As resolution and precision of analytical techniques improve, analysts need to be aware that non-atmospheric, high frequency signals are present in ice core trace gas records resulting from enrichment associated with melt layers and variability related to layered bubble trapping.

- Careful choices regarding discrete sample size and dimension, and post-processing of continuous data sets are required to avoid misinterpretation. Analysts should integrate trace gas data over multiple annual layers to smooth out the trapping signal, paying particular attention to time periods of relatively high atmospheric CH_4 growth rate. Isolated anomalous CH_4 signals should be anticipated at sites where surface melt is possible. These considerations are especially relevant for studies of the inter-polar gradient (e.g., Mitchell et al., 2013) because the absolute concentrations are so important to the conclusions reached.

1   • The magnitude of CH_4 trapping signal within an ice core record or in a time slice can

2   be predicted using a firn air transport model adapted for the purpose (Mitchell et al.,

3   2015), provided information about the local density variability at the site is known.

4   Density information from the firn could plausibly be extrapolated to Holocene ice but

5   not to ice from widely different climatic conditions. If variability in chemical

6   concentrations or impurities recorded in the ice phase could somehow be interpreted

7   as a proxy for local density variability, this could help to inform modeling efforts.

8   This study presents only an incremental step towards utilising chemistry records in

9   this way.

10 **5.2   Implications for our understanding of gas trapping**

11   • Our empirical data demonstrate that layered gas trapping is driven by highly regular

12   (seasonal) variations in the physical properties of layered firn, as suggested by

13   Martinerie et al. (1992). Whether local density or some other closely-related property

14   is primarily responsible for driving this seasonal variability in bubble occlusion is not

15   clear.

16   • The regular CH_4 oscillations of the trapping signal indicate that significant bubble

17   closure must occur in the early-closure layers above the lock-in depth. Vertical

18   diffusion though early-closure layers must be maintained for several years (our

19   observations suggest up to 20 yr) to allow relatively young air to become trapped in

20   late-closure layers below.

21   • Despite the many bubble-free layers observed in the Tunu13 ice core, we do not find

22   evidence of fully 'sealing layers' above the lock-in zone—there is no major departure

23   from the relationship between trapping signal and linear atmospheric growth rate

24   (Fig. 5). Such a layer has only been observed previously in the Law Dome DE08-2

25   ice core; this thick melt layer caused an 80% reduction in gas diffusion (Trudinger et

26   al., 1997). A recent examination of bubble-free layers in the WAIS Divide core also

27   found no evidence for significant impact on gas transport (Orsi et al., 2015).

28   • The layered bubble trapping process has the effect of broadening the *modelled* gas

29   age distribution of the air in ice cores, relative to a model scenario without layered

30   bubble trapping but the same prescribed firn air diffusivity profile. Age distributions

1   in realistic models of non-layered firn compared to layered firn that capture the effect

2   of layering on the diffusivity have yet to be studied, as far as we are aware. However,

3   in nature, the presence of firn layering presumably leads to the formation of a lock-in

4   zone, which causes a narrowing of the gas age distribution by limiting vertical

5   diffusion. The net effect of firn layering is therefore likely to be a reduction in the

6   width of the gas age distribution of air trapped in ice cores (Mitchell et al., 2015).

7 An open question generated by this study is: Why do the high frequency oscillations in

8 CH_4 concentration increase sharply in amplitude across the transition from mature ice

9 into the lock-in zone (Sect. 3.3)? The findings of Mitchell et al. (2015) suggest that

10 contamination from ambient air is relatively low in continuous data from the lock-in zone

11 and not enough to account for the 10-fold amplitude increase. So, if CH_4 variability in

12 the lock-in zone and in the mature ice phase are both related to layered bubble trapping,

13 what causes the discontinuity? Could it be that drilling and cutting the ice samples

14 inherently influences the observations by re-opening centimetre-scale pore clusters that

15 were already closed off from the atmosphere? It may be that the only way to resolve this

16 question is to devise a way to eliminate firn air alteration caused by both ambient air

17 contamination and the re-opening of pores, perhaps by analysing trace gases across the

18 lock-in zone to mature ice transition in-situ.

19

20 **Data availability**

21 Data produced by this study are available to download in the Supplement.

22

References

Alley, B., 1988. Concerning the deposition and diagenesis of strata in polar firn. J. Glaciol. 34, 283–290.

Aydin, M., Montzka, S.A., Battle, M.O., Williams, M.B., De Bruyn, W.J., Butler, J.H., Verhulst, K.R., Tatum, C., Gun, B.K., Plotkin, D.A., Hall, B.D., Saltzman, E.S., 2010. Post-coring entrapment of modern air in some shallow ice cores collected near the firn-ice transition: evidence from CFC-12 measurements in Antarctic firn air and ice cores. Atmos Chem Phys 10, 5135–5144. doi:10.5194/acp-10-5135-2010

Buizert, C., Martinerie, P., Petrenko, V.V., Severinghaus, J.P., Trudinger, C.M., Witrant, E., Rosen, J.L., Orsi, A.J., Rubino, M., Etheridge, D.M., Steele, L.P., Hogan, C., Laube, J.C., Sturges, W.T., Levchenko, V.A., Smith, A.M., Levin, I., Conway, T.J., Dlugokencky, E.J., Lang, P.M., Kawamura, K., Jenk, T.M., White, J.W.C., Sowers, T., Schwander, J., Blunier, T., 2014. Corrigendum to ``Gas transport in firn: multiple-tracer characterisation and model intercomparison for NEEM, Northern Greenland'' published in Atmos. Chem. Phys., 12, 4259–-4277, 2012. Atmos Chem Phys 14, 3571–3572. doi:10.5194/acp-14-3571-2014

Buizert, C., Martinerie, P., Petrenko, V.V., Severinghaus, J.P., Trudinger, C.M., Witrant, E., Rosen, J.L., Orsi, A.J., Rubino, M., Etheridge, D.M., Steele, L.P., Hogan, C., Laube, J.C., Sturges, W.T., Levchenko, V.A., Smith, A.M., Levin, I., Conway, T.J., Dlugokencky, E.J., Lang, P.M., Kawamura, K., Jenk, T.M., White, J.W.C., Sowers, T., Schwander, J., Blunier, T., 2012. Gas transport in firn: multiple-tracer characterisation and model intercomparison for NEEM, Northern Greenland. Atmospheric Chem. Phys. 12, 4259–4277. doi:10.5194/acp-12-4259-2012

Butler, J.H., Battle, M., Bender, M.L., Montzka, S.A., Clarke, A.D., Saltzman, E.S., Sucher, C.M., Severinghaus, J.P., Elkins, J.W., 1999. A record of atmospheric halocarbons during the twentieth century from polar firn air. Nature 399, 749–755. doi:10.1038/21586

Campen, R.K., Sowers, T., Alley, R.B., 2003. Evidence of microbial consortia metabolizing within a low-latitude mountain glacier. Geology 31, 231–234. doi:10.1130/0091-7613

Chappellaz, J., Stowasser, C., Blunier, T., Baslev-Clausen, D., Brook, E.J., Dallmayr, R., Faïn, X., Lee, J.E., Mitchell, L.E., Pascual, O., Romanini, D., Rosen, J., Schüpbach, S., 2013. High-resolution glacial and deglacial record of atmospheric methane by continuous-flow and laser spectrometer analysis along the NEEM ice core. Clim Past 9, 2579–2593. doi:10.5194/cp-9-2579-2013

Etheridge, D., Pearman, G.I., Fraser, P.J., 1992. Changes in tropospheric methane between 1841 and 1978 from a high accumulation-rate Antarctic ice core. Tellus 44B, 282–294.

Faïn, X., Chappellaz, J., Rhodes, R.H., Stowasser, C., Blunier, T., McConnell, J.R., Brook, E.J., Preunkert, S., Legrand, M., Debois, T., Romanini, D., 2014. High resolution measurements of carbon monoxide along a late Holocene Greenland ice core: evidence for in situ production. Clim Past 10, 987–1000. doi:10.5194/cp-10-987-2014

Fujita, S., Goto-Azuma, K., Hirabayashi, M., Hori, A., Iizuka, Y., Motizuki, Y., Motoyama, H., Takahashi, K., 2016. Densification of layered firn in the ice sheet at Dome Fuji, Antarctica. J. Glaciol. FirstView, 1–21. doi:10.1017/jog.2016.16

Fujita, S., Hirabayashi, M., Goto-Azuma, K., Dallmayr, R., Satow, K., Zheng, J., Dahl-Jensen, D., 2014. Densification of layered firn of the ice sheet at NEEM, Greenland. J. Glaciol. 60, 905–921. doi:10.3189/2014JoG14J006

Gregory, S.A., Albert, M.R., Baker, I., 2014. Impact of physical properties and accumulation rate on pore close-off in layered firn. The Cryosphere 8, 91–105. doi:10.5194/tc-8-91-2014

Hörhold, M.W., Kipfstuhl, S., Wilhelms, F., Freitag, J., Frenzel, A., 2011. The densification of layered polar firn. J. Geophys. Res. 116, F01001. doi:10.1029/2009jf001630

Hörhold, M.W., Laepple, T., Freitag, J., Bigler, M., Fischer, H., Kipfstuhl, S., 2012. On the impact of impurities on the densification of polar firn. Earth Planet. Sci. Lett. 325-326, 93–99. doi:10.1016/j.epsl.2011.12.022

Hou, S., Chappellaz, J., Raynaud, D., Masson-Delmotte, V., Jouzel, J., Bousquet, P., Hauglustaine, D., 2013. A new Himalayan ice core CH4 record: possible hints at the preindustrial latitudinal gradient. Clim. Past 9, 2549–2554. doi:10.5194/cp-9-2549-2013

Jones, S.J., 1967. Softening of ice crystals by dissolved fluoride ions. Phys. Lett. A 25, 366–367. doi:10.1016/0375-9601(67)90702-5

Keegan, K., Albert, M.R., Baker, I., 2014. The impact of ice layers on gas transport through firn at the North Greenland Eemian Ice Drilling (NEEM) site, Greenland. The Cryosphere 8, 1801–1806. doi:10.5194/tc-8-1801-2014

Klein, K., 2014. Variability in dry Antarctic firn—Investigations on spatially distributed snow and firn samples from Dronning Maud Land, Antarctica. PhD thesis, University of Bremen, Bremen, Germany.

MacFarling Meure, C., Etheridge, D., Trudinger, C., Steele, P., Langenfelds, R., van Ommen, T., Smith, A., Elkins, J., 2006. Law Dome CO2, CH4 and N2O ice core records extended to 2000 years BP. Geophys. Res. Lett. 33, doi:10.1029/2006GL026152.

Martinerie, P., Raynaud, D., Etheridge, D.M., Barnola, J.-M., Mazaudier, D., 1992. Physical and climatic parameters which influence the air content in polar ice. Earth Planet. Sci. Lett. 112, 1–13. doi:10.1016/0012-821X(92)90002-D

McConnell, J.R., Aristarain, A.J., Banta, J.R., Edwards, P.R., Simões, J.C., 2007. 20th-Century doubling in dust archived in an Antarctic Peninsula ice core parallels climate change and desertification in South America. Proc. Natl. Acad. Sci. 104, 5743–5748.

McConnell, J.R., Lamorey, G.W., Lambert, S.W., Taylor, K.C., 2002. Continuous ice-core chemical analyses using inductively coupled plasma mass spectrometry. Environ. Sci. Technol. 36, 7–11. doi:10.1021/es011088z

Mitchell, L., Brook, E., Lee, J.E., Buizert, C., Sowers, T., 2013. Constraints on the Late Holocene anthropogenic contribution to the atmospheric methane budget. Science 342, 964–966. doi:10.1126/science.1238920

Mitchell, L.E., Brook, E.J., Sowers, T., McConnell, J.R., Taylor, K., 2011. Multidecadal variability of atmospheric methane, 1000-1800 C.E. J. Geophys. Res. 116, doi:10.1029/2010JG001441. doi:10.1029/2010jg001441

Mitchell, L.E., Buizert, C., Brook, E.J., Breton, D.J., Fegyveresi, J., Baggenstos, D., Orsi, A., Severinghaus, J., Alley, R.B., Albert, M., Rhodes, R.H., McConnell, J.R., Sigl, M., Maselli, O., Gregory, S., Ahn, J., 2015. Observing and modeling the influence of layering on bubble trapping in polar firn. J. Geophys. Res. Atmospheres 120, 2558–2574. doi:10.1002/2014JD022766

Morville, J., Kassi, S., Chenevier, M., Romanini, D., 2005. Fast, low-noise, mode-by-mode, cavity-enhanced absorption spectroscopy by diode-laser self-locking. Appl. Phys. B Lasers Opt. 80, 1027–1038.

Nakamura, T., Jones, S.J., 1970. Softening effect of dissolved hydrogen chloride in ice crystals. Scr. Metall. 4, 123–126. doi:10.1016/0036-9748(70)90176-6

NEEM community members, 2013. Eemian interglacial reconstructed from a Greenland folded ice core. Nature 493, 489–494.

Neftel, A., Oeschger, H., Schwander, J., Stauffer, B., 1983. Carbon dioxide concentration in bubbles of natural cold ice. J. Phys. Chem. 87, 4116–4120. doi:10.1021/j100244a025

NGRIP community members, 2004. High-resolution record of Northern Hemisphere climate extending into the last interglacial period. Nature 431, 147–151.

Orsi, A.J., Kawamura, K., Fegyveresi, J.M., Headly, M.A., Alley, R.B., Severinghaus, J.P., 2015. Differentiating bubble-free layers from melt layers in ice cores using noble gases. J. Glaciol. 61, 585–594.

Priscu, J.C., Hand, K.P., 2010. Microbial habitability of icy worlds. Microbe Mag. Am. Soc. Microbiol.

Rasmussen, S.O., Abbott, P.M., Blunier, T., Bourne, A.J., Brook, E., Buchardt, S.L., Buizert, C., Chappellaz, J., Clausen, H.B., Cook, E., Dahl-Jensen, D., Davies, S.M., Guillevic, M., Kipfstuhl, S., Laepple, T., Seierstad, I.K., Severinghaus, J.P., Steffensen, J.P., Stowasser, C., Svensson, A., Vallelonga, P., Vinther, B.M., Wilhelms, F., Winstrup, M., 2013. A first chronology for the North Greenland Eemian Ice Drilling (NEEM) ice core. Clim Past 9, 2713–2730. doi:10.5194/cp-9-2713-2013

Rhodes, R.H., Brook, E.J., Chiang, J.C., Blunier, T., Maselli, O.J., McConnell, J.R., Romanini, D., Severinghaus, J.P., 2015. Enhanced tropical methane production in response to iceberg discharge in the North Atlantic. Science 348, 1016–1019.

Rhodes, R.H., Faïn, X., Stowasser, C., Blunier, T., Chappellaz, J., McConnell, J.R., Romanini, D., Mitchell, L.E., Brook, E.J., 2013. Continuous methane measurements from a late Holocene Greenland ice core: Atmospheric and in-situ signals. Earth Planet. Sci. Lett. 368, 9–19. doi:10.1016/j.epsl.2013.02.034

Rohde, R.A., Price, P.B., Bay, R.C., Bramall, N.E., 2008. In situ microbial metabolism as a cause of gas anomalies in ice. Proc. Natl. Acad. Sci. 105, 8667–8672. doi:10.1073/pnas.0803763105

Rosen, J.L., Brook, E.J., Severinghaus, J.P., Blunier, T., Mitchell, L.E., Lee, J.E., Edwards, J.S., Gkinis, V., 2014. An ice core record of near-synchronous global climate changes at the Bølling transition. Nat. Geosci. 7, 459–463. doi:10.1038/ngeo2147

Sander, R., 2015. Compilation of Henry's law constants (version 4.0) for water as solvent. Atmospheric Chem. Phys. 15, 4399–4981. doi:10.5194/acp-15-4399-2015

Schwander, J., Barnola, J.M., Andrié, C., Leuenberger, M., Ludin, A., Raynaud, D., Stauffer, B., 1993. The age of the air in the firn and the ice at Summit, Greenland. J. Geophys. Res. 98, 2831–2838. doi:10.1029/92jd02383

Schwander, J., Sowers, T., Barnola, J.M., Blunier, T., Fuchs, A., Malaizé, B., 1997. Age scale of the air in the summit ice: Implication for glacial-interglacial temperature change. J. Geophys. Res. 102, 19483–19493. doi:10.1029/97jd01309

Severinghaus, J.P., Albert, M.R., Courville, Z.R., Fahnestock, M.A., Kawamura, K., Montzka, S.A., Mühle, J., Scambos, T.A., Shields, E., Shuman, C.A., Suwa, M., Tans, P., Weiss, R.F., 2010. Deep air convection in the firn at a zero-accumulation site, central Antarctica. Earth Planet. Sci. Lett. 293, 359–367. doi:10.1016/j.epsl.2010.03.003

Sigl, M., Winstrup, M., McConnell, J.R., Welten, K.C., Plunkett, G., Ludlow, F., Büntgen, U., Caffee, M., Chellman, N., Dahl-Jensen, D., Fischer, H., Kipfstuhl, S., Kostick, C., Maselli, O.J., Mekhaldi, F., Mulvaney, R., Muscheler, R., Pasteris, D.R., Pilcher, J.R., Salzer, M., Schüpbach, S., Steffensen, J.P., Vinther, B.M., Woodruff, T.E., 2015. Timing and climate forcing of volcanic eruptions for the past 2,500 years. Nature 523, 543–549. doi:10.1038/nature14565

Sowers, T., Bender, M., Raynaud, D., Korotkevich, Y.S., 1992. δ15N of N2 in air trapped in polar ice: A tracer of gas transport in the firn and a possible constraint on ice age-gas age differences. J. Geophys. Res. Atmospheres 97, 15683–15697. doi:10.1029/92JD01297

Spahni, R., Schwander, J., Fluckiger, J., Stauffer, B., Chappellaz, J., Raynaud, D., 2003. The attenuation of fast atmospheric CH4 variations recorded in polar ice cores. Geophys. Res. Lett. 30, 1571. doi:10.1029/2003gl017093

Stowasser, C., Buizert, C., Gkinis, V., Chappellaz, J., Schüpbach, S., Bigler, M., Faïn, X., Sperlich, P., Baumgartner, M., Schilt, A., Blunier, T., 2012. Continuous measurements of methane mixing ratios from ice cores. Atmospheric Meas. Tech. 5, 999–1013. doi:10.5194/amt-5-999-2012

Sturrock, G.A., Etheridge, D.M., Trudinger, C.M., Fraser, P.J., Smith, A.M., 2002. Atmospheric histories of halocarbons from analysis of Antarctic firn air: Major Montreal Protocol species. J. Geophys. Res. Atmospheres 107, 4765. doi:10.1029/2002JD002548

Trudinger, C.M., Enting, I.G., Etheridge, D.M., Francey, R.J., Levchenko, V.A., Steele, L.P., Raynaud, D., Arnaud, L., 1997. Modeling air movement and bubble trapping in firn. J. Geophys. Res. Atmospheres 102, 6747–6763. doi:10.1029/96JD03382

Weiler, K., 2008. On the composition of firn air and its dependence on seasonally varying atmospheric boundary conditions and the firn structure. PhD thesis, University of Bern, Bern, Switzerland.

Table 1. Locations, site characteristics and other relevant information for ice cores

featured in this study. Please refer to footnotes for explanation of abbreviations.

Ice core & location (see map Fig. S1)	Depth interval (m)	Gas age interval (yrAD)	Δage and FWHM (yr)	Accum. rate (cm ice yr⁻¹)	Mean annual temp. (°C)	Mean liq. cond. (μS)	Age scale
B40 Drønning Maud Land, E. Antarctica 75.001ºS, 0.068ºE 2911 m elevation	200–88	331–1710	811 65	6.8[b]	-46[b]	1.33	Ice: ALC+VS Gas: tied to WDC06A-7[f]
D4 S. Central Greenland 71.40ºN, 43.08ºW 2,713 m elevation	146–61	1825–1961	90 14	41	-24	101	Ice: ALC+VS Gas: tied to WDC06A-7[f] & Law Dome[g]
NEEM NW Greenland 77.45ºN, 51.06ºW 2,450 m elevation	573–399	-682–322	187[a] 17	22[c]	-28.9[c]	122	Ice: GICC05[h] Gas: GICC05[h]
NGRIP Central Greenland 75.10ºN, 42.32ºW 2,917 m elevation	569–519 254–207 108–74	-929–-616 980–1237 1780–1926	235 18	19[d]	-31.5[d]	122 105 107	Ice: GICC05[h] Gas: tied to WDC06A-7[f]
Tunu13 NE Greenland 78.035ºN, 33.879ºW 2,200 m elevation	213–73	836–1893	314–369 21–27	10–14	-29[e]	115	Ice: ALC+VS[i] Gas: tied to WDC06A-7[f]
WAIS Divide West Antarctica 79.47ºS, 112.08ºW 1766 m elevation	n/a	n/a	208[j]	20[j]	-31[j]	n/a	n/a

3   Footnotes:

4   Δage = difference between gas age and ice age. If no reference is provided, value is estimated by age scale
5   synchronisation or OSU firn air model.

6   FWHM= Full Width at Half Maximum of gas age distribution at close-off depth estimated by OSU firn air
7   model (Rosen et al., 2014).

8   Mean liq. cond. = mean liquid conductivity value for ice core analysed

9   ALC=annual layer count; VS=volcanic synchronisation

10   Gas age scales do not incorporate lock-in zone measurements.
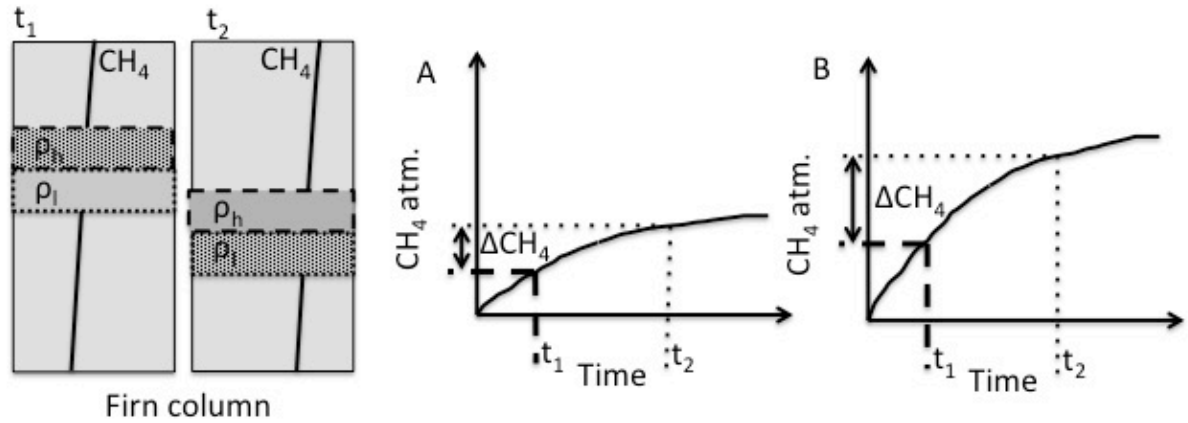
11   References:

12   a=(Buizert et al., 2014); b=(Klein, 2014); c=(NEEM community members, 2013); d=(NGRIP community
13   members, 2004); e=(Butler et al., 1999); f=(Mitchell et al., 2013); g=(MacFarling Meure et al., 2006);
14   h=(Rasmussen et al., 2013); i=(Sigl et al., 2015); j=(Mitchell et al., 2011)

1 Table 2. Discrete CH_4 and total air content measurements on Tunu13 samples containing

2 melt layers. Estimated CH_4 concentrations of the melt layers result from a simple mixing

3 calculation using air content measurements made on Summit melt layer samples. Values

4 in parentheses reflect the range of melt layer air content values measured. Predicted CH_4

5 values are calculated using the assumption that the melt layer was in equilibrium with the

6 atmosphere, according to Henry's Law (0ºC, 0.750 atm.). Henry's Law constants for

7 CH_4, O_2 and N_2 were obtained from NIST Chemistry WebBook (webbook.nist.gov).

8 CH_4 concentrations of adjacent samples are used as atmospheric concentrations at time of

9 melt layer formation. All of these samples are from the Tunu13 Main core.

| Sample depth range (m)	Sample CH_4 conc. (ppb)	Sample total air content (cm^3/g ice STP)	Melt layer thickness (mm)	Estimated CH_4 conc. of melt layer (ppb)	x-fold CH_4 enrichment of ML relative to sample	Mean CH_4 conc. of adjacent samples (ppb)	Predicted CH_4 conc. of melt layer in equilib. with atmos. (ppb)
113.910–113.970	773.6	0.0956	4.0	6355 (4781–9940)	8.6	737.1	1492
153.225–153.300	730.3	0.0859	4.0	1829 (1519–2533)	2.5	723.9	1465
156.235–156.285	744.1	0.0941	4.0	5356 (4076–8356)	7.4	721.0	1460
181.710–181.760	700.3	0.0970	4.0	2539 (2020–3721)	3.7	686.1	1389
194.610–194.700	771.9	0.0847	24.0	3683 (2842–5596)	5.4	684.0	1385

10

1

2   Figure 1.: Schematic to illustrate how the layered bubble trapping mechanism can

3   generate high frequency CH_4 artifacts in ice cores. At time t_1, air bubbles within the

4   relatively high density (p_h) layer are closed off at a relatively shallow depth in the firn

5   column. At time t_2, air bubbles with the relatively low density (p_l) layer are closed off

6   deeper in the firn column. Between t_1 and t_2 the atmospheric concentration of CH_4 is

7   increasing and so the CH_4 concentration in the diffusive column also increases,

8   generating a CH_4 concentration difference ΔCH_4 between the bubbles in depth-adjacent

9   layers trapped at t_1 and t_2. Increasing the atmospheric CH_4 growth rate (B compared to

10   A) results in a larger ΔCH_4. A negative atmospheric growth rate would cause a change in

11   the sign of ΔCH_4.

1
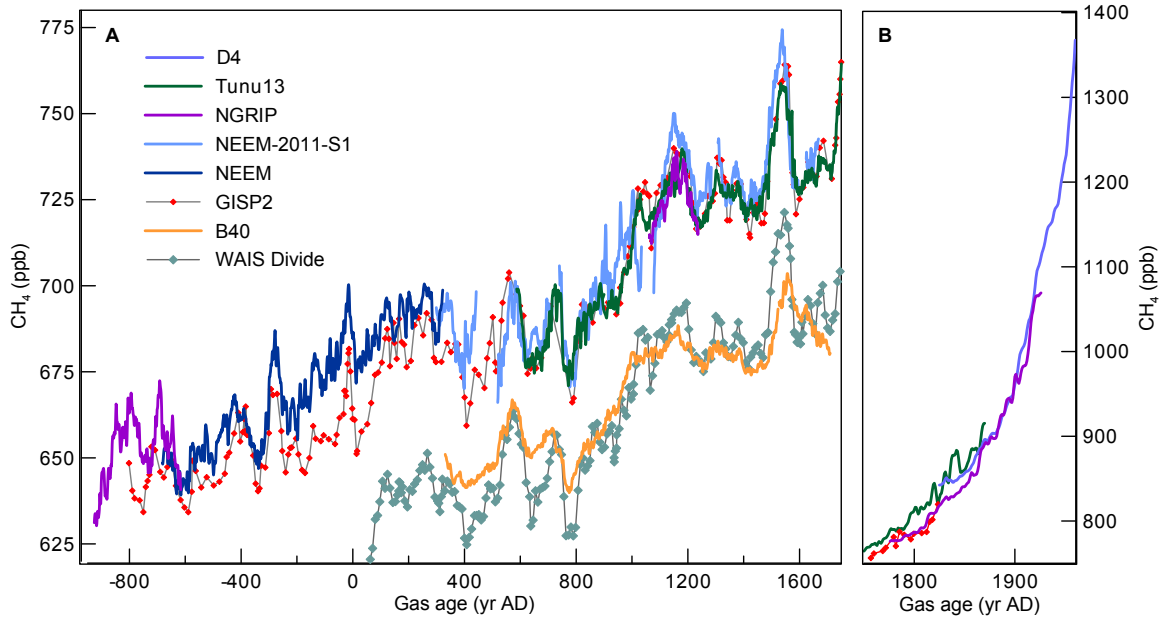
2

3 Figure 2. Late Holocene continuous CH_4 data from Tunu13, D4, NGRIP and NEEM

4 Greenland ice cores and B40 Antarctic ice core for time periods -900–1750 AD (A) and

5 1750–1960 AD (B). Each record is a cubic spline fit with 1 yr sample spacing to the 5 s

6 integrated data. No data from the lock-in zone are included on this figure. Also plotted

7 are discrete CH_4 data from GISP2 and WAIS Divide ice cores (Mitchell et al., 2013) and

8 NEEM-2011-S1 continuous CH_4 data (Rhodes et al., 2013).
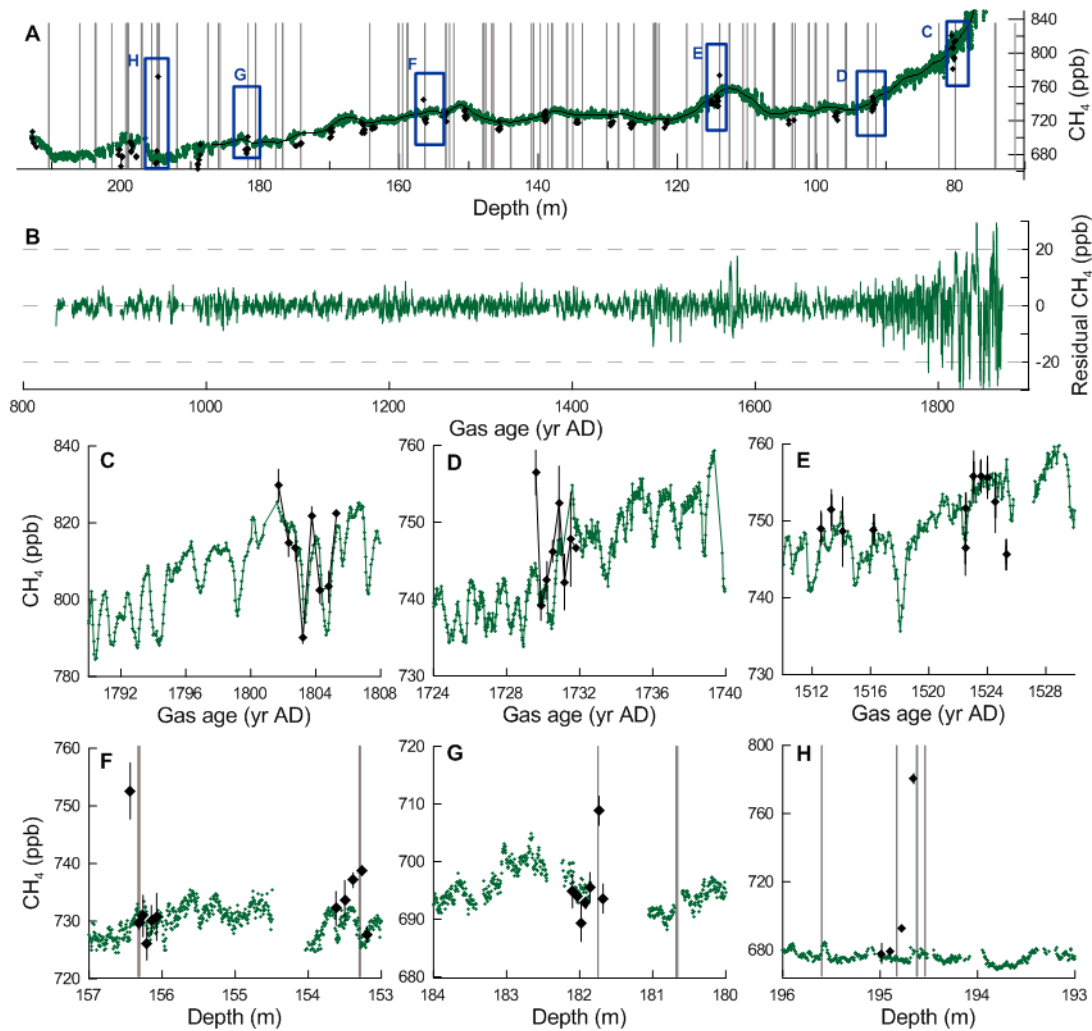
Figure 3. Decimetre-scale CH_4 variability in Tunu13 mature ice captured by continuous (green) and discrete (black diamonds) analyses: A) Both records on depth scale with vertical grey lines indicating depths of bubble-free layers observed; B) Residual high frequency non-atmospheric component of Tunu13 signal: continuous record from panel A (green) minus cubic spline fit (black line on panel A). Older data from below 172 m depth are excluded because there are too many data gaps resulting from poor core quality. Y-axis has been clipped at -30 and +30 ppb. Data minimum and maximum are -38 and 36 ppb; C, D & E) Zoomed views of high frequency CH_4 variability within blue rectangles displayed on panel A; F, G & H) Zoomed views of anomalously high discrete CH_4 concentrations associated with melt layers. CH_4 concentrations of discrete data points are increased by 8.5 ppb on panels C-H to aid comparison with online data. 2 σ internal precision uncertainty bars are plotted for discrete data. Horizontal bars on

1   discrete measurements represent depth interval of each sample. Depth uncertainty for the

2   continuous data is estimated to be ± 2 cm (2 σ).
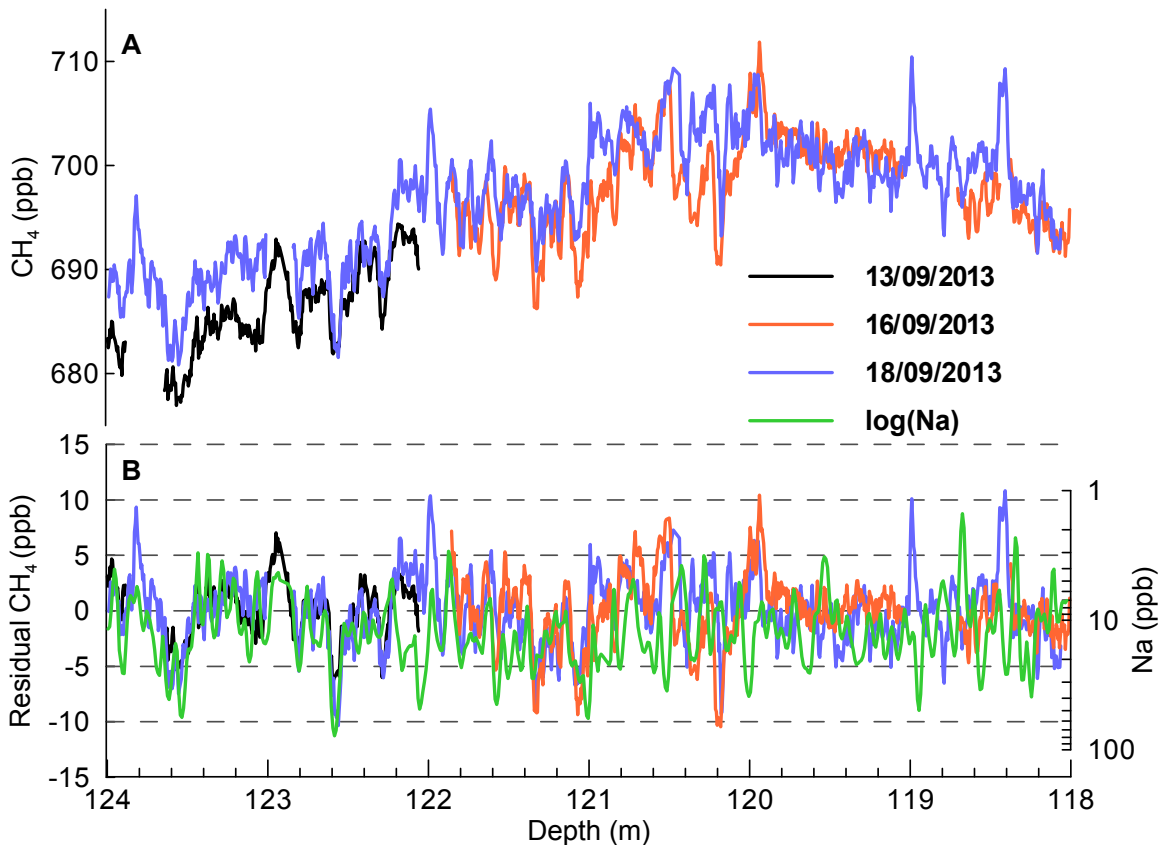
Figure 4. High frequency CH_4 variability in B40 (E. Antarctica) ice. Measured signals (A) and the residual (signal − spline fit) (B) are shown. Variability is replicated by analyses performed on the three dates displayed in legend (dd/mm/yyyy). Gas extraction was performed using a Membrana micromodule degasser on 13/09/2013 and an IDEX in-line degasser on 16/09/2013 and 18/09/2013 (Table S1). Although it is difficult to be certain that anomalously high CH_4 spikes are not the result of ambient air entry at the melterhead, the anomalously low troughs cannot be analytical artifacts. Also shown on panel B is Na concentration, which typically co-varies with Cl concentration. Many of the anomalously low CH_4 values are coincident in depth with relatively high Na. This depth interval is dated as 1493–1583 AD gas age.
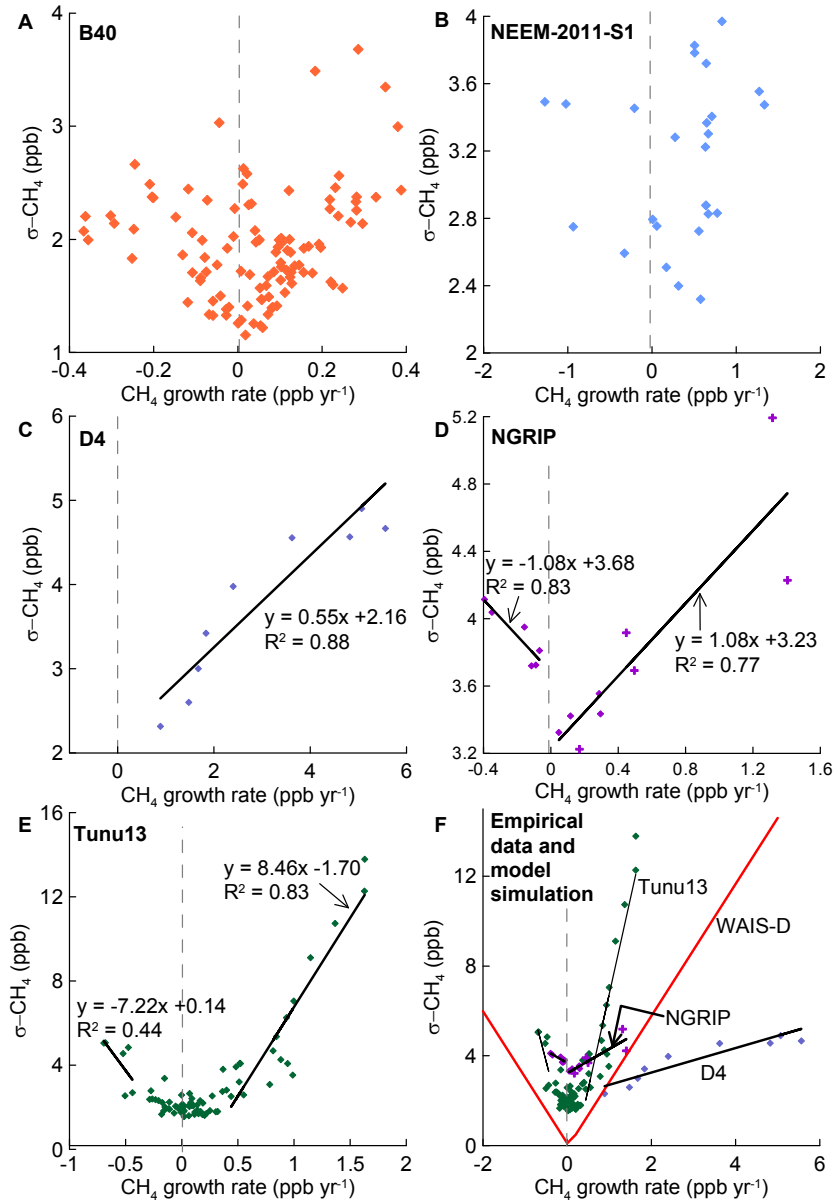
Figure 5. Relationship between CH_4 growth rate and high frequency CH_4 variability (σ-CH_4) in the following ice cores: B40 (A), NEEM-2011-S1 (B), D4 (C), NGRIP (D), Tunu13 (E). σ-CH_4 is calculated every 10 yr for intervals of 40 yr duration (except for 5 NGRIP data points (cross symbols), which are discrete 10 yr intervals with no overlap, due to poor core quality and discontinuous record). Linear regression of growth rate and σ-CH_4 is displayed where appropriate. A linear fit is applied to Tunu13 and D4 data with growth rates $> \pm 0.4$ ppb yr^{-1} and to NGRIP data with growth rates $> \pm 0.1$ ppb yr^{-1}. Panel F displays data from Tunu13, D4 and NGRIP with firn air transport model output for the WAIS Divide ice core.
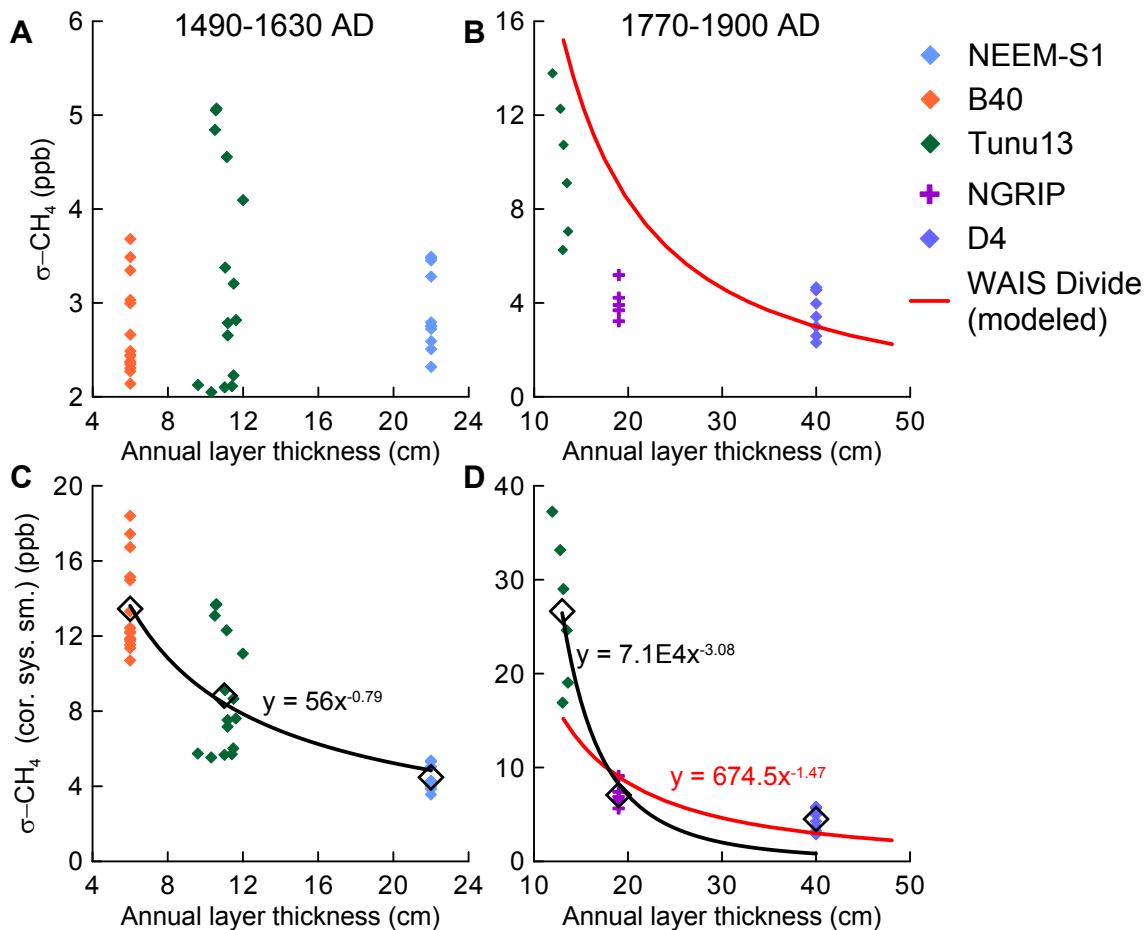
Figure 6. Relationship between accumulation rate and high frequency CH_4 variability.
The vertical panels represent two time intervals: 1490–1630 AD (A) and 1770–1900 AD
(B) for which high resolution CH_4 data are available from three ice cores with different
accumulation rates. Note that the three clusters of data points for each time period do not
represent the same ice cores in each case. The top row (A & B) displays CH_4 standard
deviation (σ) about the long-term spline. Values are calculated every 10 yr for intervals
of 40 yr duration as Fig. 5 (except for NGRIP data points on B&D that represent discrete
10 yr intervals). The bottom row (C & D) displays σ-CH_4 values adjusted (increased by
1.25–5 depending on ice core) to correct for the damping effect of the continuous
analytical system (Fig. S2). Mean values for each ice core on each panel are displayed
(black diamonds) with power law relationships (black line). Also shown is the
relationship between accumulation rate and σ-CH_4 for WAIS Divide (at 2.5 ppb yr^{-1}
atmospheric growth rate) as predicted by the CIC firn air transport model.
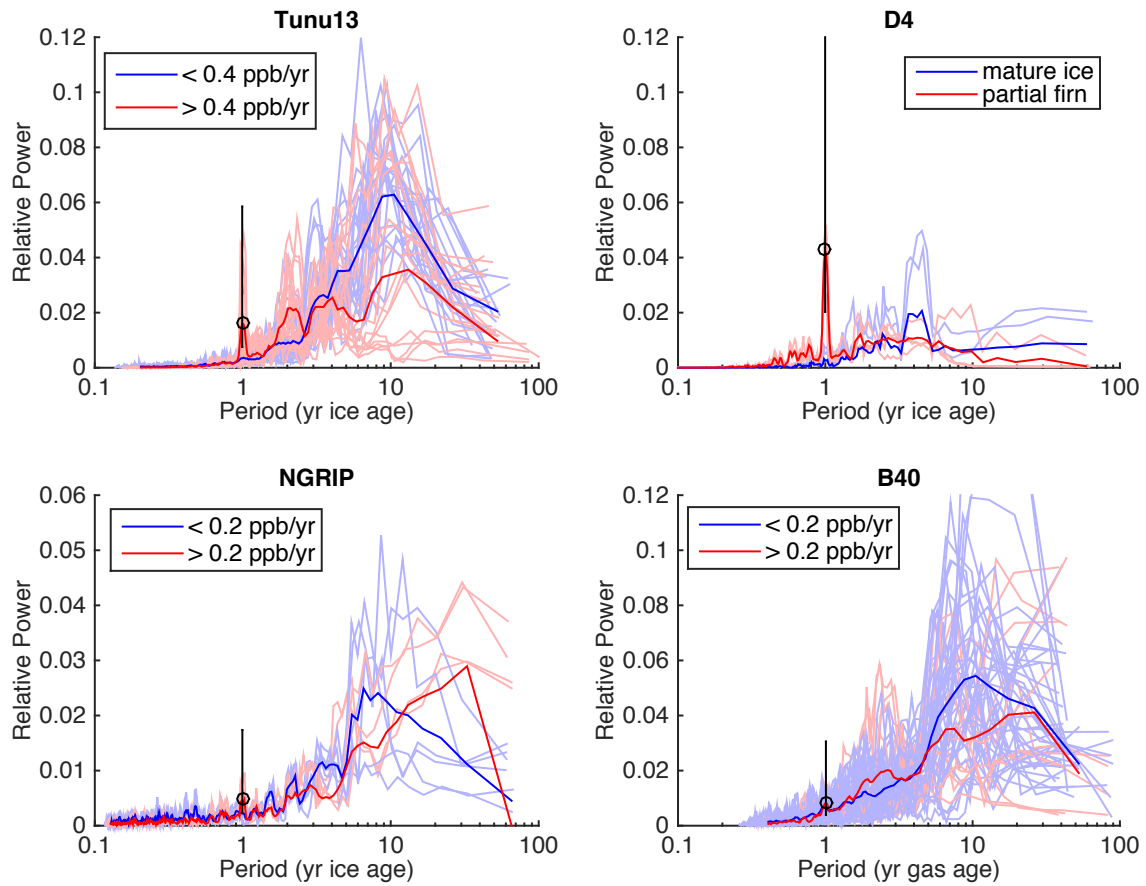
Figure 7. Multi-taper method (MTM) spectra of high frequency, non-atmospheric residual CH_4 variability of four ice cores. MTM was performed in the ice age domain using 2 tapers and 3 degrees of freedom. Each spectrum represents a 40 yr window of data. For Tunu13, NGRIP and B40 each spectrum is colour-coded according to the CH_4 growth rate of that data window. For D4, spectra are colour-coded according to whether or not the time window encompasses data from the lock-in zone (< 82 m depth). All D4 spectra represent time windows of CH_4 growth rate > 0.4 ppb yr^{-1}. The bold lines represent averaged spectra for the low/high growth rate or mature ice/partial firn categories. Black open circles represent the mean relative power at 1 yr period. Vertical lines represent 90% confidence intervals for the averaged spectra (bold, red lines only) based on a chi-squared distribution. Spectral peaks are significant for Tunu13 and D4 because the confidence interval exceeds the background spectral noise.
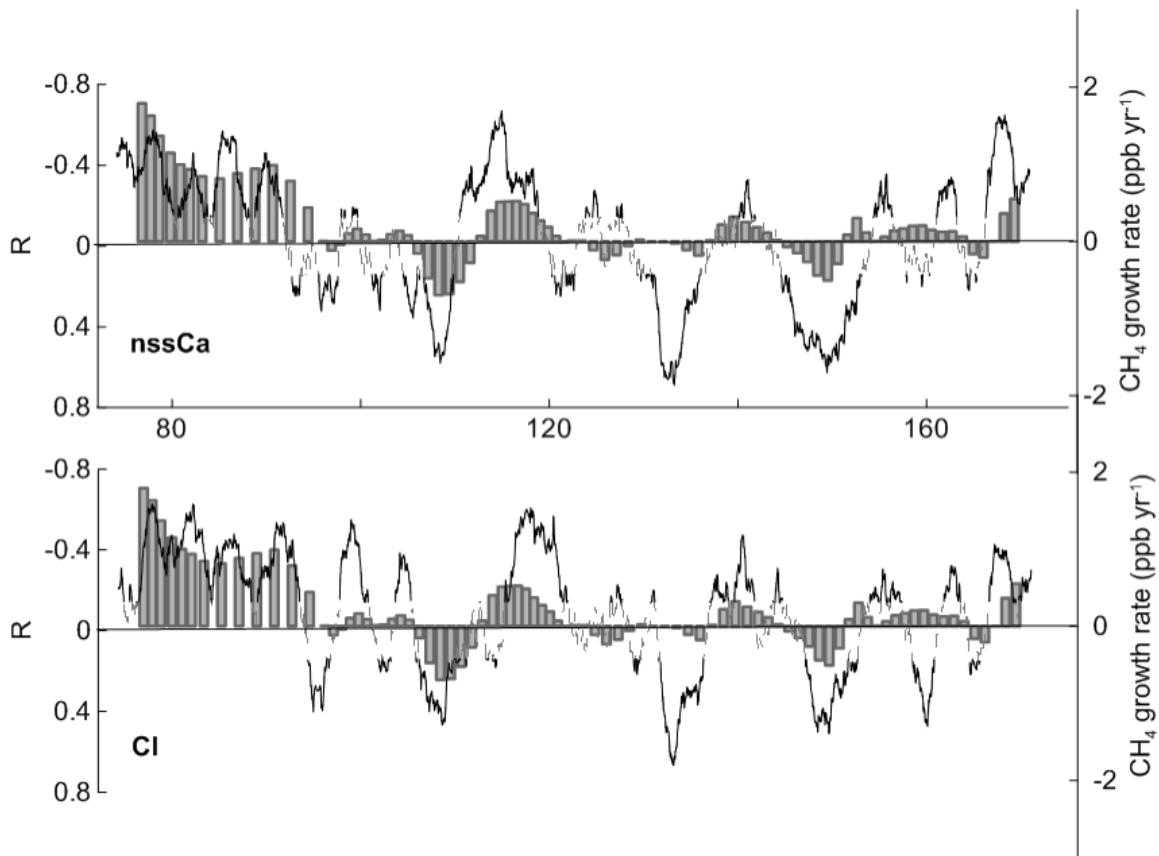
Figure 8. Moving window Spearman's rank correlation between concentrations of non-sea salt (nss) Ca and Cl and σ-CH_4 in the Tunu13 ice core (line) compared to CH_4 growth rate (vertical bars). Note the reverse direction of the left-hand y-axes. Significant ($p < 0.05$) (solid line) and non-significant (grey dashed line) coefficient of correlation (R) values are plotted. Correlation is calculated for non-overlapping, 2 m length windows (using 0.5–5 m length windows produces similar results). The σ-CH_4 time series is resampled to the depth spacing of chemistry data (1 cm) so $n = 200$ for each window.